Impact of the number of planetary gears on the energy efficiency of electrified powertrains

Rajput, Daizy; Herreros, Martin; Innocente, Mauro S.; Bryans, Jeremy; Schaub, Joschka; Dizqah, Arash M.

DOI:
10.1016/j.apenergy.2022.119531

Document Version
Publisher's PDF, also known as Version of record

Citation for published version (Harvard):
Rajput, D, Herreros, M, Innocente, MS, Bryans, J, Schaub, J & Dizqah, AM 2022, 'Impact of the number of planetary gears on the energy efficiency of electrified powertrains', *Applied Energy*, vol. 323, 119531. https://doi.org/10.1016/j.apenergy.2022.119531

Applied Energy 323 (2022) 119531

Contents lists available at ScienceDirect

Applied Energy

journal homepage: www.elsevier.com/locate/apenergy

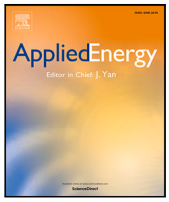

Impact of the number of planetary gears on the energy efficiency of electrified powertrains

Daizy Rajput [a,b,*], Jose M. Herreros [c,d], Mauro S. Innocente [a,b], Jeremy Bryans [b], Joschka Schaub [e], Arash M. Dizqah [c,f]

[a] Autonomous Vehicles & Artificial Intelligence Laboratory (AVAILAB), UK
[b] Centre for Future Transport and Cities (CFTC), Coventry University, Coventry CV1 5FB, UK
[c] Smart Vehicles Control Laboratory (SVeCLab), UK
[d] University of Birmingham, Birmingham B15 2TT, UK
[e] FEV Europe GmbH, Neuenhofstraße 181, 52078 Aachen, Germany
[f] University of Sussex, Brighton BN1 9RH, UK

ARTICLE INFO

Keywords:
Hybrid electric vehicle
Energy management strategy
Optimal control
Automotive simulation models
dSPACE
AMPL
Neos server
Gearbox

ABSTRACT

Planetary gears (PGs) play a critical role in hybrid electric vehicles (HEVs) by combining the output torques of different powertrain components and delivering the resulting torque to the wheels. Whilst previous studies show that the number of planetary gears affects performance of HEVs, there is no prior study to systematically investigate such effects on energy consumption. This paper quantifies the energy efficiency improvement of HEVs due to increasing the number of PGs from one to two, and from two to three. This is done by comparing the minimum energy consumption for different topologies when the rest of the powertrain components – namely electric motors, batteries and engine – are the same. To calculate the minimum energy consumption, the paper proposes an optimal energy management strategy (EMS) for each topology to find the optimum sequence of clutch engagement and torque distribution. The minimum energy consumption of a vehicle with different number of PGs is then evaluated using the automotive simulation models (ASM) from dSPACE. Results show that, for the same electric motors and engine, increasing the number of PGs from one to two and from two to three reduces energy consumption by 5% and 1.5%, respectively.

1. Introduction

In 2020, the UK government issued a strict 95 g/km limit on the CO_2 emission for all ground vehicles to address the global concern of pollution control [1]. A further 15% decrease is expected by year 2025. Automotive industries have been investing in hybrid electric powertrains to reduce fuel consumption and achieve these ambitious targets. Performance of a hybrid powertrain depends on the efficiency of its components as well as on its topology, number of planetary gears (PGs), and associated energy management strategies (EMSs).

The topology of hybrid powertrains is one of the critical factors that affect fuel consumption [2–4]. Topology refers to the way that the powertrain components – namely engine, motors, and differential – are connected to the wheels. There are three well-known topologies which are widely used in hybrid powertrains: series, parallel, and power-split. The latter is a parallel topology that consists of one or more PGs as power splitters, thus providing better fuel economy [5]. Toyota Prius, Chevrolet Volt, and Ford Fusion Hybrid are among the first to launch power-split topologies with one PG. Adding a clutch to the traditional Toyota Prius powertrain with one PG is shown to reduce the total energy consumption by 2.6% [6]. A power-split powertrain that includes clutches is called a multi-mode topology, which provides better fuel economy than the traditional single-mode topologies due to the higher degrees of freedom (DoF) over a wider range of operating conditions [7].

Increasing the number of PGs also appears to reduce energy consumption of a power-split powertrain. For example, Rajput et al. [8] reported a 4% decrease in energy consumption by increasing the number of PGs from one to two. Benefiting from the reduction in total fuel consumption, Toyota and General Motors launched hybrid powertrains with two PGs for their Prius [9] and Chevrolet Volt [10] models, respectively. Later, Zhuang et al. [3] showed that increasing from two to three PGs further reduces the total energy consumption by 1.1% due to the introduction of new modes of operation. However, this increment is limited by the fact that the powertrain components are not identical

* Corresponding author at: Centre for Future Transport and Cities (CFTC), Coventry University, Coventry CV1 5FB, UK.
E-mail address: rajputd@uni.coventry.ac.uk (D. Rajput).

https://doi.org/10.1016/j.apenergy.2022.119531
Received 1 April 2022; Received in revised form 27 May 2022; Accepted 18 June 2022
Available online 20 July 2022

Nomenclature

r_{tyre}	Tyre radius
m_{ice}	Engine fuel consumption
m_{eqv}	Equivalent fuel consumption
m_t	Total energy consumption
$bsfc$	Brake specific fuel consumption
ω_R	Angular velocity of ring gear
ω_S	Angular velocity of sun gear
ω_C	Angular velocity of carrier gear
ω_{out}	Angular velocity of output shaft
T_{mg1}	Torque of motor generator 1
T_{mg2}	Torque of motor generator 2
T_e	Torque of engine
η_{mg1}	Efficiency of motor generator 1
η_{mg2}	Efficiency of motor generator 2
η_{bth}	Brake thermal efficiency of engine
T_{req}	Torque requested by vehicle
m	Mass of vehicle
$C_{\tau_{mg2}}$	Torque constant MG2
$C_{\tau_{mg1}}$	Torque constant MG1
R_{mg2}	MG2 Resistance
R_{mg1}	MG1 Resistance
P_{batt}	Battery power
C_{batt}	Capacity (i.e., charge) of battery (kWh)
M_i	Mode$_i$
I_*	Inertia of powertrain components
ω_*	Angular velocity of powertrain components
R_i	Radius of ring gear of i-PG topology
S_i	Radius of sun gear of i-PG topology
F_i	Internal force acting between gears of i-PG topology
SoC	State of charge
k	Number of sample
T_k	Sampling time
q	Fuel flow rate of engine
ρ	Density of gasoline
Q_{HHV}	Calorific value of gasoline
α	Motor states −1 for motoring and 0 for regeneration
P_{max}	Maximum power
T_{max}	Maximum torque
SP_{max}	Maximum speed

for different topologies. Moreover, the engagement and disengagement of clutches are not penalised even though this is known to increase mechanical losses [11]. General Motors (GM) introduced a 3PG powertrain topology, referred to as 2-Mode Hybrid Transmission, for applications involving full acceleration, hill climbing, and towing [12].

The aforementioned studies investigated the performance of commercial hybrid electric vehicles (HEVs) with one, two, and three PGs – referred to as 1PG, 2PG, and 3PG topologies from here forth – and not the explicit effect of increasing the number of PGs on energy consumption. The analysis of the latter requires evaluating the performance of the topologies when the power components are identical and optimally operating. Therefore, the comparison relies on the development of an optimal EMS for each topology to choose the best mode, configuration, and torque distribution over the driving cycle to minimise energy consumption and CO_2 emission.

Each mode of operation of a power-split powertrain represents a type of configuration, which is defined as a topology with a particular order of clutch engagements. A power-split hybrid topology with multiple clutches can generate numerous configurations, some of which may belong to the same mode of operation. For example, a hybrid powertrain may operate at the fully electric mode – where only electric machines contribute to the torque of the wheels – whilst this mode of operation can be realised with different configurations.

There is an extensive list of previously developed EMSs for hybrid powertrains, including rule-based strategies [13]; online optimisation-based strategies [14–18]; equivalent consumption minimisation strategy (ECMS) [19–21]; Pontryagin's minimum principle-based strategies [22]; learning-based EMSs [23–25]; predictive EMSs [26]; and Hierarchical EMSs [27]. Moreover, researchers have proposed a so-called deep reinforcement learning (DRL) based energy and emission management strategy (E&EMS), and results show that two distributed DRL algorithms improved the learning efficiency of the E&EMS by four times [28,29]. These EMSs either are only suitable for single-mode topologies or provide a sub-optimal solution by decoupling mode selection and torque distribution actions.

The contributions of this paper to address these gaps are as follows:

- Evaluation of the impact of number of PGs on the energy consumption of HEVs. It is shown that increasing the number of PGs from one to two and from two to three reduces the energy consumption by 5% and 1.5%, respectively.
- Optimal EMS for the multi-mode hybrid electric powertrains with different numbers of PGs. The developed EMS simultaneously controls the clutches of the gearbox as well as energy flows of components to minimise energy consumption over a driving cycle.
- Design rules are introduced for HEVs with multiple PGs:
    1. Electric motors with higher speed give flexibility to improve the engine efficiency and therefore reduce energy consumption. This can happen by both the 2PG and 3PG topologies.
    2. Engine can operate within the optimum range of its rotational speed using the fixed-gear modes and without involvement of electric motors. This is possible in 3PG topologies and reduces the electric losses and hence the energy consumption.

The main motivation of this paper is to develop a test environment to evaluate the sensitivity of the performance of the electrified powertrain with respect to only one design variable that is the number of PGs. The proposed EMS makes the evaluation valid by finding the optimal energy consumption of different topologies, which nullifies the effect of other design variables.

The remainder of this paper is organised as follows: the system components are presented in Section 2; the developed EMS is described in Section 3; the real-time simulation results are discussed in Section 4; whilst conclusions are drawn in Section 5.

2. System components

This paper studies the impact of five multi-mode topologies on the energy consumption of a nominal hybrid electric passenger car. This includes four topologies introduced by Toyota, Chevrolet and General Motors, and an additional one proposed in Zhuang et al. [30], on the energy consumption of a nominal hybrid electric passenger car. Throughout this paper, these hybrid topologies are referred to as 1PG-1, 2PG-1, 2PG-2, 3PG-1, and 3PG-2. Table 1 summarises the size of the components and other parameters of the nominal car that hosts the five transmissions. The developed models of the system components are summarised below, whilst more details are provided in Appendices A and B.

Table 1
Sizes of the powertrain components.

Component name	Parameters
Engine	$P_{e,\max}$ = 50 kW at 4500 rpm, $T_{e,\max}$ = 105 Nm at 2000 rpm, η_{bth} = 33% at 2050 rpm, refer Fig. 8b for the bsfc map of the engine.
Motor generator 2	$P_{mg2,\max}$ = 60 kW, $T_{mg2,\max}$ = ±200 Nm, $SP_{mg2,\max}$ = ±13,000 rpm, refer Fig. 8a for the efficiency map of the MG2.
Motor generator 1	$P_{mg1,\max}$ = 42 kW, $T_{mg1,\max}$ = ±200 Nm, $SP_{mg1,\max}$ = ±30,000 rpm, refer Fig. 8c for the efficiency map of the MG1.
Battery capacity	$P_{batt,\max}$ = 27 kWh, C_{10} = 6.5 Ah, R_{int} = 0.5 Ω
PG1 ratio	
R_1:S_1	2.6
PG2 ratio	
R_1:S_1	2.6
R_2:S_2	2.63
PG3 ratio	
R_1:S_1	2
R_2:S_2	2
R_3:S_3	2
Differential gear ratio	3.95
Vehicle mass	1450 kg
Tyre radius	0.33 m

Table 2
List of modes generated by different topologies. Degrees of freedom are with respect to the component speeds.

Mode	Symbol	Topologies	Description
1	m_1	1PG-1 2PG-1 2PG-2 3PG-1 3PG-2	EV mode (2 × MGs, 0 × DoF)
2	m_2	2PG-2 3PG-1 3PG-2	Parallel with fixed-gear mode (1 × MG+engine, 0 × DoF)
3	m_3	1PG-1 2PG-1 2PG-2 3PG-1 3PG-2	Input-split mode (1 × MG+engine, 1 × DoF)
4	m_4	1PG-1 2PG-1 2PG-2 3PG-1 3PG-2	EV mode (1 × MG, 0 × DoF)
5	m_5	2PG-2 3PG-1	Compound split mode (Flexible combination, 1 × DoF)
6	m_6	3PG-1 3PG-2	Parallel with fixed-gear mode (2 × MGs+engine, 0 × DoF)
7	m_7	3PG-2	Parallel with fixed-gear mode (2 × MG+engine, 0 × DoF)
8	m_8	1PG-1 2PG-1	Series mode (1 × MG and 1 × MG+engine, 1 × DoF)
9	m_9	2PG-2 3PG-1 3PG-2	Parallel with fixed-gear mode (1 × MG, 0 × DoF)

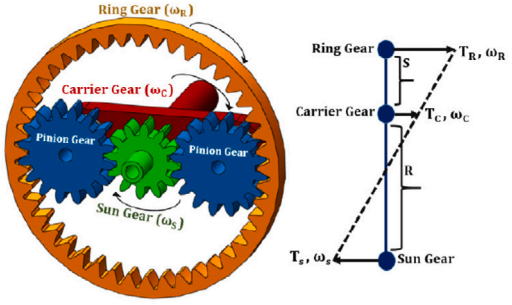

Fig. 1. 3-D representation of a planetary gearbox and its lever analogy [8].

Table 3
Clutch engagements of all topologies in Fig. 2 to realise different modes, where CL_i+CL_j means that clutches i and j are the only ones engaged to generate the mode whilst N.A. means that the corresponding mode-topology pairing is not available.

Modes	Topologies				
	1PG-1	2PG-1	2PG-2	3PG-1	3PG-2
Mode 1 (m_1)	CL_1+CL_3	CL_1+CL_3	CL_1+CL_3	CL_3	CL_1
Mode 2 (m_2)	N.A.	N.A.	CL_1+CL_2	CL_1+CL_2	CL_1+CL_2
Mode 3 (m_3)	CL_1	CL_1	CL_2	CL_1	CL_1
Mode 4 (m_4)	CL_2+CL_3	CL_2+CL_3	CL_2+CL_3	CL_2	CL_1
Mode 5 (m_5)	N.A.	N.A.	CL_1	CL_1+CL_3	CL_2
Mode 6 (m_6)	N.A.	N.A.	N.A.	CL_2+CL_3	CL_1+CL_4
Mode 7 (m_7)	N.A.	N.A.	N.A.	N.A.	CL_2+CL_4
Mode 8 (m_8)	CL_3	CL_3	N.A.	N.A.	N.A.
Mode 9 (m_9)	N.A.	N.A.	N.A.	CL_1+CL_2+CL_3	N.A.

2.1. Planetary gearset

One or more PGs are in the core of the power-split hybrid powertrains. As shown in Fig. 1, a PG consists of three gears, namely the sun (S), ring (R), and carrier (C) gears. The radii of the ring and sun gears are referred to as R_r and S_s, respectively. However, a PG only has two degrees of freedom because the angular velocities of these three gears are related as follows:

$$\omega_S S_s + \omega_R R_r = \omega_C (R_r + S_s) \tag{1}$$

Fig. 2 shows a lever diagram of each of the five hybrid topologies considered in this study. Table 2 also summarises all the modes of operation that these topologies can generate. Fig. 2(a) shows the 1PG topology, which can realise three modes of operation with different clutch engagements. Figs. 2(b) and 2(c) show 2PG-1 and 2PG-2 topologies, respectively, which can realise up to five modes. Figs. 2(d) and 2(e) show the 3PG-1 and 3PG-2 topologies, respectively, which can generate up to seven modes of operation.

Each mode of operation is modelled by a binary variable indicating whether the mode is selected. For example, m_1 = 1 means that Mode 1 is selected. Evidently, only one mode can be selected at any one time.

Zhang et al. [9] introduced an automated process to formulate the behaviour of the gearbox at each mode of operation. For example, the behaviour of the 1PG topology when operating in m_1, m_3 and m_4 is represented by (2), (3) and (4), respectively.

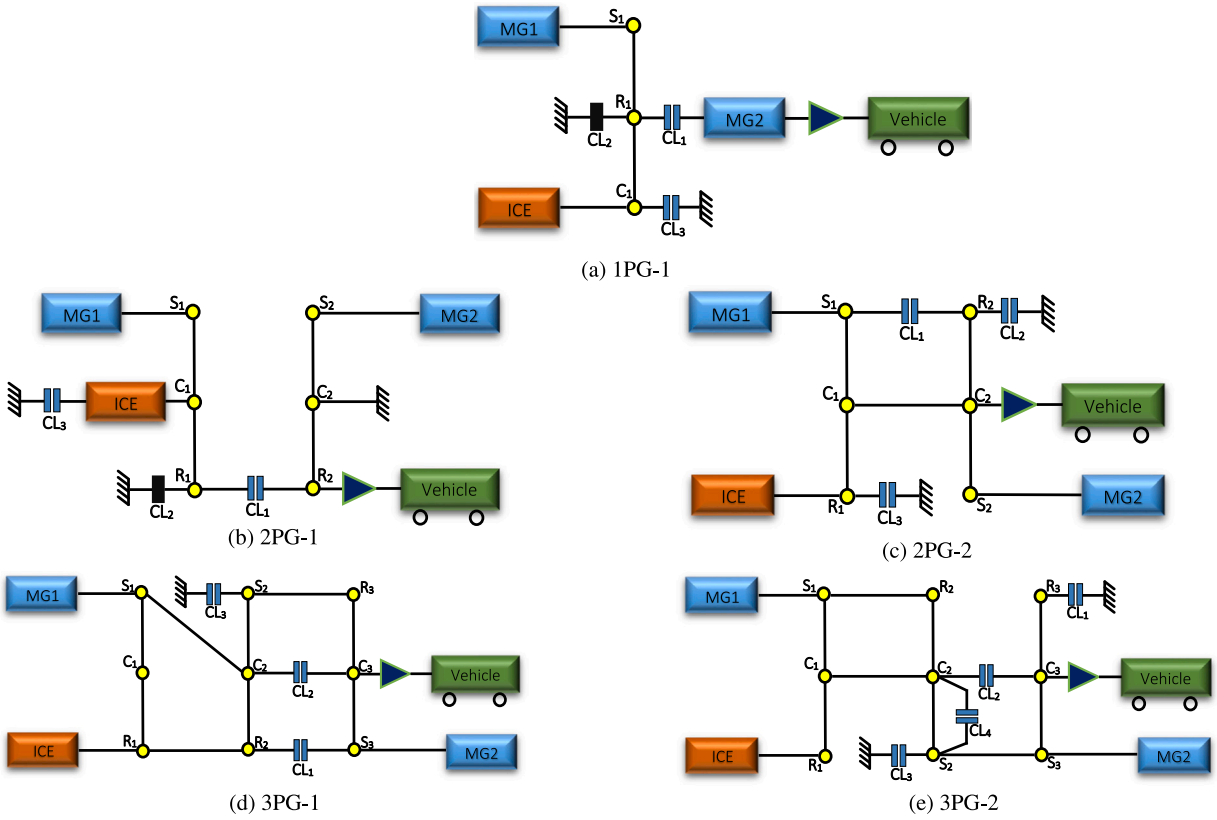

Fig. 2. Topologies used in this study: (a) 1PG-1, (b) 2PG-1, (c) 2PG-2, (d) 3PG-1, (e) 3PG-2. The solid black box represents the engaged clutch whilst the two thick blue lines represent disengaged clutches.

1. Mode 1 — EV mode (2×MGs, 0×DoF)

$$\begin{bmatrix} \frac{mr_{tyre}^2}{K^2} + I_{mg2} & 0 & -R_1 \\ 0 & I_{mg1} & S_1 \\ -R_1 & S_1 & 0 \end{bmatrix} \begin{bmatrix} \dot{\omega}_{out} \\ \dot{\omega}_{mg1} \\ F_1 \end{bmatrix} = \begin{bmatrix} T_{mg2} - \frac{T_{req}}{D_{GR}} \\ T_{mg1} \\ 0 \end{bmatrix} \tag{2}$$

2. Mode 3 — Input-split mode (1×MG + engine, 1×DoF)

$$\begin{bmatrix} I_e & 0 & 0 & R_1 + S_1 \\ 0 & \frac{mr_{tyre}^2}{K^2} + I_{mg2} & 0 & -R_1 \\ 0 & 0 & I_{mg1} & -S_1 \\ R_1 + S_1 & -R_1 & -S_1 & 0 \end{bmatrix} \begin{bmatrix} \dot{\omega}_e \\ \dot{\omega}_{out} \\ \dot{\omega}_{mg1} \\ F_1 \end{bmatrix} = \begin{bmatrix} T_e \\ T_{mg2} - \frac{T_{req}}{D_{GR}} \\ T_{mg1} \\ 0 \end{bmatrix} \tag{3}$$

3. Mode 4 — EV mode (1×MG, 0×DoF)

$$\left(\frac{mr_{tyre}^2}{K^2} + I_{mg2} \right) \dot{\omega}_{out} = T_{mg2} - \left(\frac{T_{req}}{D_{GR}} \right) \tag{4}$$

2.2. Electric motors

The hybrid powertrain in this study includes two electric motors which share the same torque characteristics but differ in their power and speed profiles. Motor-Generator 1 (MG1) operates as the engine speed controller in all modes, while it contributes towards the total torque request in m_1 and m_6 only. Motor-Generator 2 (MG2) is the only source of power in m_4, and the primary source of electric power in all other modes. MG2 is also used for regeneration in all topologies.

The electric motors in this study are modelled with their efficiency maps at different values of mechanical torque and rotational speed. The efficiency map of the electric motor $i \in \{1, 2\}$, which depends on the internal resistance and torque constant of the motor, is represented as in (5).

$$\eta_{mg_i} = \left(\frac{1}{1 + \frac{\left(T_{mg_i}/C_{T_{mg_i}}\right)^2 R_{mg_i}}{T_{mg_i}\omega_{mg_i}}} \right), \; i \in \{1, 2\} \tag{5}$$

2.3. Engine

The hybrid powertrain of this study uses a gasoline engine which is attached to different gears of the PGs depending on the topology. As shown in Fig. 2, the engine is connected to the carrier gear of the first PG (C_1) in both 1PG-1 and 2PG-1 topologies, whereas it is connected to the ring gear of the first PG (R_1) in the remaining topologies. In order to make a fair comparison, all topologies use the same engine, which is represented as a map of its brake-thermal efficiency in terms of rotational speed and mechanical torque:

$$\eta_{bth} = \frac{\pi T_e}{\rho q Q_{HHV}} \tag{6}$$

The fuel flow rate of the engine (q_k) is measured in mm^3/cycle and modelled as a polynomial of degree five (quintic function) in terms of the engine torque and angular velocity. For further details on this polynomial, refer to Appendix B.

2.4. Battery

The state of charge (SoC) of batteries is a function of time, and of their charging and discharging power. This is modelled by the following ordinary differential equation (ODE):

$$SoC_{k+1} = SoC_k - T_k\left(\frac{P_{\text{batt},k}}{3600 \cdot C_{\text{batt}}}\right) \tag{7}$$

where $P_{batt,k} > 0$ shows that the battery is being discharged. The sampling time of the driving cycles is normally one second (i.e. $T_k = 1$).

The battery power is a hybrid algebraic function (i.e. a function of both continuous and discontinuous variables) of torque, angular velocity, and efficiency of MG1 and MG2:

$$P_{\text{batt}} = T_{\text{mg1}}\omega_{\text{mg1}}\eta_{mg1}^{\gamma_1} + T_{\text{mg2}}\omega_{\text{mg2}}\eta_{\text{mg2}}^{\gamma_2} \tag{8}$$

where $\gamma_1, \gamma_2 \in \{-1, 1\}$ are binary variables that, respectively, indicate whether MG1 and MG2 are in the motoring ($\gamma_i = -1$) or generating ($\gamma_i = 1$) mode of operation. Both the MG1 and MG2 are used for motoring in mode 1 whereas MG2 is the only source of electric traction in modes 2–8. Without loss of generality, it is assumed that only MG2 performs regeneration.

3. Energy Management Strategy (EMS)

For an unbiased study, the energy consumption of hybrid powertrains with different numbers of PGs must be compared operating optimally over the driving cycle. Therefore, we propose here an EMS that performs both mode selection and torque distribution simultaneously to ensure optimal operation of the powertrain over the given cycle. An EMS with simultaneous mode selection and torque distribution leads to a complex mixed-integer optimisation problem due to the existence of discontinuities caused by changing the mode of operation; i.e. due to engaging and disengaging clutches and switching the operation of the electric motors between motoring and generating. This fact, along with the nonlinearity of components and the existence of algebraic constraints, results in the EMS comprising a mixed-integer nonlinear optimal control problem (OCP) with differential and algebraic equations (DAEs):

$$\mathbf{u}^*(.) = \arg\min_{\mathbf{u}(.)} \sum_{k=0}^{N} J(\mathbf{x}_k, \mathbf{z}_k, \mathbf{u}_k; \theta_k) \tag{9a}$$

$$\text{s.t. :} \quad (19)\text{–}(23)$$

$$0 \le m_{p,k} \perp m_{q,k} \ge 0, \quad \forall p \ne q \in \{1..9\} \tag{9b}$$

$$\sum_{p=1}^{9} m_{p,k} = 1 \tag{9c}$$

$$F_i\left(\mathbf{x}_k, \mathbf{z}_k, \mathbf{u}_k; \theta_k\right) = 0 \tag{9d}$$

$$\underline{\mathbf{u}} \le \mathbf{u}_k \le \overline{\mathbf{u}} \tag{9e}$$

$$\underline{\mathbf{x}} \le \mathbf{x}_k \le \overline{\mathbf{x}} \tag{9f}$$

$$\underline{\mathbf{z}} \le \mathbf{z}_k \le \overline{\mathbf{z}} \tag{9g}$$

$$i \in \{\text{1PG-1, 2PG-1, 2PG-2, 3PG-2, 3PG-1}\} \tag{9h}$$

where the decision variables are the engine torque, MG2 torque, MG1 angular velocity, modes and α, and therefore $\mathbf{u} = [T_e, T_{mg2}, \omega_{mg1}, m_1, m_2, m_3, m_4, m_5, m_6, m_7, \alpha]^T$. Binary variable α represents the states of the electric motors, where $\alpha = 0$ during regeneration and $\alpha = 1$ during motoring. The battery SoC is a differential state variable: $\mathbf{x} = [SoC]$. The algebraic variables of the problem are MG1 torque, MG2 angular velocity and engine angular velocity, and therefore $\mathbf{z} = [T_{mg1}, \omega_{mg2}, \omega_e]^T$. The parameters used in this problem are the torque demand τ_{req} and the vehicle longitudinal speed $V_{vehicle}$, and therefore $\theta = [T_{req}, V_{vehicle}]$. N is the prediction horizon, which is equal to the length of the driving cycle in seconds since the sampling time T_k is one second.

The objectives of the EMS are to minimise (1) energy consumption, (2) number of mode shifts, and (3) deviation of the battery SoC from its initial value (SoC_0). This is turned into a single-objective optimisation problem by a convex combination of some quantification of each objective:

$$J = \sum_{k=0}^{N}\left\{\beta_m\dot{m} + \beta_s\dot{s}_k + \beta_{soc}(\text{SoC}_0 - \text{SoC}_k)^2\right\} \tag{10}$$

where $[\beta_m, \beta_s, \beta_{soc}] = [0.5, 0.1, 0.4]$ are the optimum convex combination coefficients for 1PG topology, which are calculated by trial and error. $\dot{m}_{t_k}$ is the rate of energy consumption. The Second and third terms of the cost functions are two soft constraints to smoothen the fluctuation of clutch engagement and to prevent deep discharge of battery.

$$\dot{m}_{t,k} = \dot{m}_{\text{e},k} + \dot{m}_{\text{eqv},k} \tag{11}$$

and:

$$\dot{m}_{\text{e},k} = \frac{q\rho\omega_{\text{e},k}}{120} \tag{12}$$

$$\dot{m}_{\text{eqv},k} = \begin{cases} \frac{T_{\text{mg2},k}\omega_{\text{mg2},k}}{\eta_{mg2,k}\eta_{\text{char}}/\eta_{\text{dischar}}}\frac{1}{0.35\text{Q}_{\text{HHV}}}m_{i,k}\alpha_k & \text{if } m \in \{2, 3, \ldots, 9\}; \\ \frac{\eta_{\text{char}}}{\eta_{\text{dischar}}}\frac{1}{0.35\text{Q}_{\text{HHV}}}m_{1,k}\alpha_k\left(\frac{T_{\text{mg2},k}\omega_{\text{mg2},k}}{\eta_{\text{mg2},k}} + \frac{T_{\text{mg1},k}\omega_{\text{mg1},k}}{\eta_{\text{mg1},k}}\right) & \text{otherwise.} \end{cases} \tag{13}$$

Minimising $\dot{s}_k$ in (14) leads to minimising the number of mode shifts. Frequent mode shifts in the hybrid powertrain will lead to excessive mechanical losses due to repeated engagement and disengagement of clutches.

$$\dot{s}_k = \frac{1}{2}\delta\gamma\left(I_{\text{e}}\left[\omega_{\text{e},k} - \omega_{\text{e},k-1}\right]^2 + I_{\text{mg1}}\left[\omega_{\text{mg1},k} - \omega_{\text{mg1},k-1}\right]^2\right) \tag{14}$$

where γ is a weighting factor fixed to 0.02 [31]. The mode change factor $\delta = 0$ when the next and current modes are the same, whilst $\delta = 1$ otherwise.

Eqs. (9b) and (9c) represent the multi-mode operation of the powertrain. The discontinuities due to the gearbox and electric motor operations are modelled by complementarity constraints (9b), where the operator $\perp$ indicates that at least one of the bounds is active (i.e. either $m_{j,k}$ or $m_{l,k}$ is zero at each time k). Eq. (9c) ensures that only one of the eight modes is active at any given k.

Eq. (9d) models each powertrain topology as a set of DAEs to characterise the behaviour of the transmission system and constraints of the power flows. Appendix A provides details of these models, where all equations are extracted from the models in Section 2.1 under steady-state conditions. For example, the steady-state equations for the 1PG topology in mode 1 (i.e. when $\dot{\omega}_e = \dot{\omega}_{out} = \dot{\omega}_{mg1} = 0$) are as follows:

$$-R_1F_1 = T_{\text{mg2}} - \frac{T_{\text{req}}}{\text{D}_{\text{GR}}} \tag{15}$$

$$S_1F_1 = T_{\text{mg1}}. \tag{16}$$

Combining Eqs. (15) and (16) to eliminate F_1, the following algebraic constraint of torques is obtained:

$$T_{\text{mg2}} = \frac{-T_{\text{mg1}}R_1}{S_1} + \frac{T_{\text{req}_k}}{D_{\text{GR}}}, \tag{17}$$

which is only valid when the powertrain operates in mode 1 and the electric motors are in traction mode; i.e. $m_1 = 1$ and $\alpha = 1$. Therefore, (17) is rewritten as a mixed-integer algebraic constraint in (18) (see also (19a) in Appendix A).

$$T_{mg2_k} = \left(\frac{-T_{mg1_k}R_1}{S_1}\alpha_k + \frac{T_{req_k}}{D_{GR}}\right)m_{1,k} \tag{18}$$

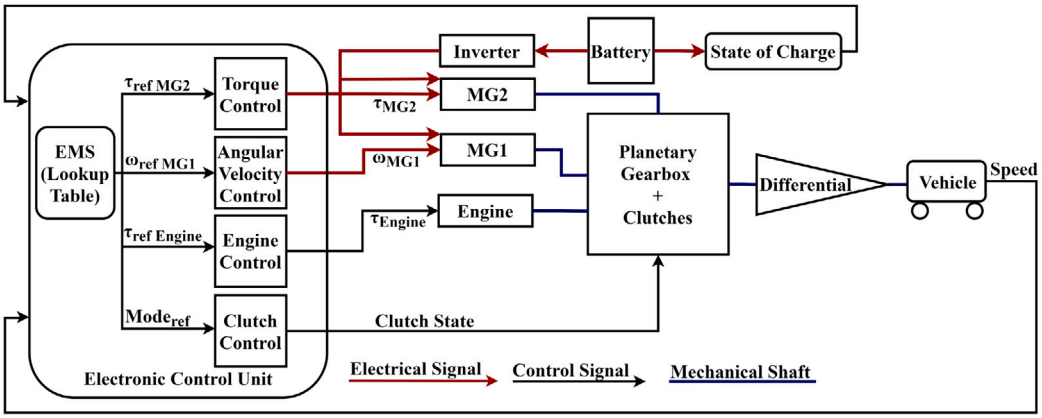

Fig. 3. A generic layout of the developed real-time simulation models using dSPACE ASM library. Planetary gearbox, EMS (as lookup table) and part of the inner controllers are specific to each topology.

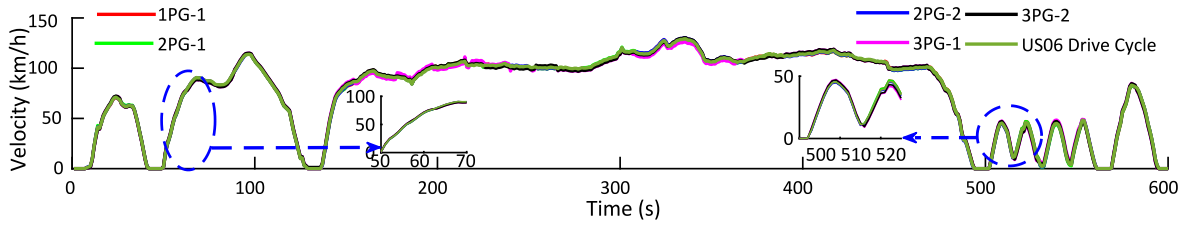

Fig. 4. Real-time simulation results showing the tracking error with respect to the desired velocity profile. The rms values of tracking error for 3PG-1 and 3PG-2 topologies are 14.23 m/s and 12.76 m/s which are higher than the corresponding values of 1PG and 2PG topologies.

The EMS in (9) is discretised and then formulated as a mixed-integer non-linear programming (MINLP) problem using the mathematical programming language (AMPL), which is the modelling language adopted by Neos server as the standard interface for solvers. The formulated problem is then solved with Knitro, available in the Neos server, which achieves a local optimal solution at every sampling time. The reliability of the solution of the EMS is assessed by using a real-time simulator which takes into account a full vehicle model and the environmental disturbances.

4. Real-time simulation

The real-time simulation models of the five hybrid topologies considered in this paper were developed based on the ASM from dSPACE. As shown in Fig. 3, the models consist of vehicle dynamics, an internal combustion engine, planetary gearbox including clutches, final drive, two motor-generators labelled MG1 and MG2, batteries and electronics, inner controllers, and the EMS developed in Section 3. The developed models are simulated over the United States 06 (US06) drive cycle with 80% initial battery SoC and a one-second sampling time. Different topologies may differ in:

1. The number of PGs in the planetary gearbox block, which varies between one and three;
2. The EMS, which is specific to each topology, solved offline, and stored as a lookup table in the ECU.

The ECU also contains inner controllers for the torques of MG2 and engine, the angular velocity of MG1, and the gearbox clutches.

4.1. Results and discussion

Fig. 4 shows the tracking performance of the developed powertrain with 1PG-1, 2PG-1, 2PG-2, 3PG-1, and 3PG-2 topologies. The root mean square values of tracking error for 3PG-1 and 3PG-2 topologies are

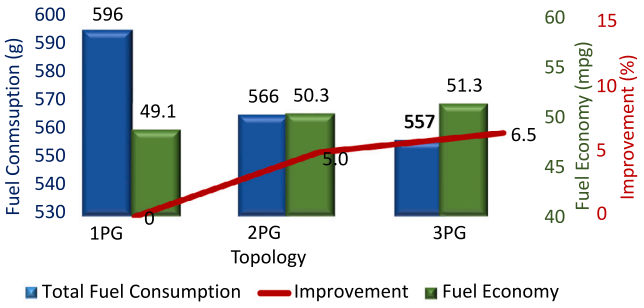

Fig. 5. Comparison of total fuel consumption, fuel economy, and reduction percentage of fuel consumption for topologies with different numbers of PGs over US06 drive cycle.

14.23 m/s and 12.76 m/s, respectively. The corresponding tracking errors for the 1PG-1, 2PG-1, and 2PG-2 topologies are 8.22 m/s, 10.05 m/s, and 11.65 m/s, respectively. In other words, the speeds of the vehicle with 3PG topologies deviates more than the other topologies from the desired profile. This is due to the fact that 3PG topologies introduce more number of modes of operation and hence more clutch fluctuations adding the complexity of the soft ECU, clutch, and drivetrain models of the real-time simulation models, which increases the resulting tracking error of speed. More precisely, there are 7 modes in 3PG-1 and 6 modes in 3PG-2 topologies, compared to 4 modes in 1PG and 5 modes in 2PG topologies.

Table 4 shows the energy consumption of each of the topologies over the US06 drive cycle. The total fuel consumption is the sum of the fuel consumption by the engine and the equivalent fuel consumption by the electric motors. The equivalent fuel consumption is the amount of burned fuel to recharge the battery through MG1 to its initial SoC (80%) after completing the driving cycle and with the engine operating at its optimal point.

The total fuel consumption of the 1PG-1 topology is 596 g whereas that of the 2PG-1 topology is 566 g (i.e. 5.0% lower). Moving from

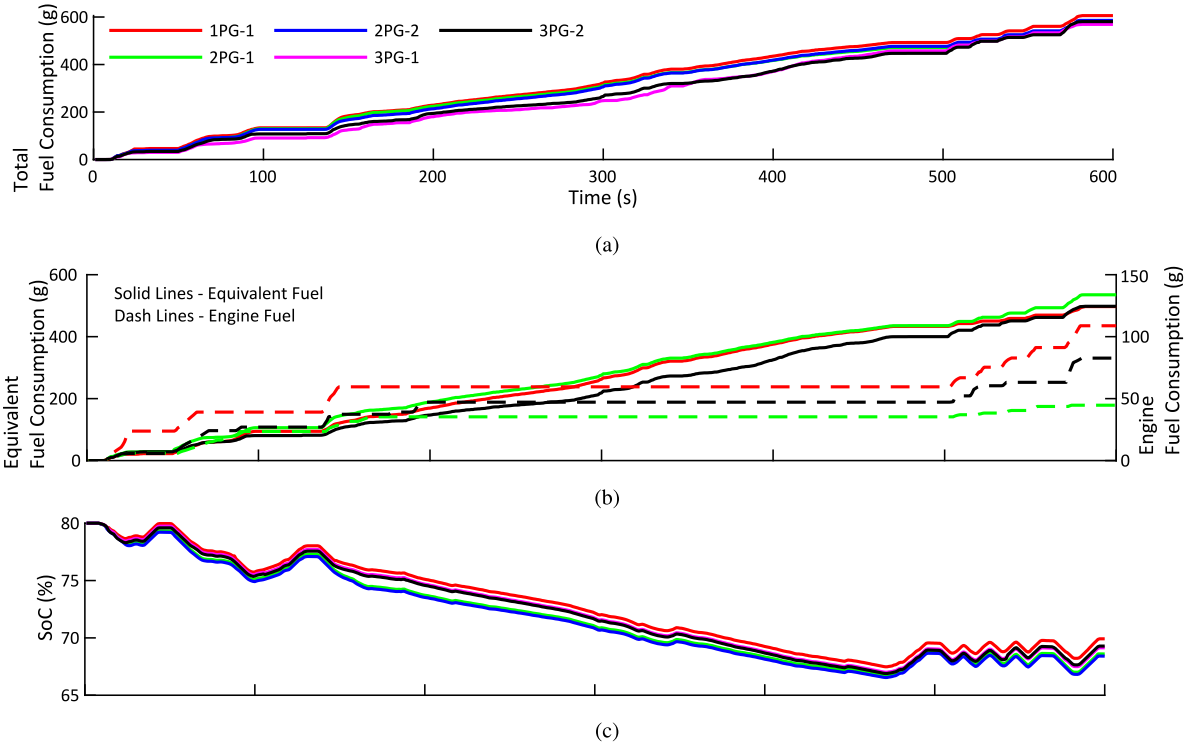

Fig. 6. Variations of the (a) total fuel consumption, (b) equivalent and engine fuel consumption and (c) SoC of battery for 1PG-1, 2PG-1 and 3PG-2 topologies.

Table 4
Summary of the real-time simulation results over US06 drive cycle.

Description	1PG-1	2PG-1	2PG-2	3PG-1	3PG-2
Total fuel consumption	596 g	566 g	588 g	579 g	557 g
Total engine fuel consumption	101 g	33.8 g	50 g	71 g	54.2 g
Total equivalent fuel consumption	495 g	532.2 g	538 g	508 g	502.8 g
Battery SoC at the end of cycle	70.2%	68.6%	68.3%	69.1%	69.3%

2PG to 3PG can reduce the total fuel consumption by a further 1.5% (i.e. 6.5% lower than that of the 1PG topology). As shown in Table 4, the 2PG-2 and 3PG-1 topologies also reduce fuel consumption with respect to the 1PG-1 topology by 1.3% and 2.8%, respectively. Engine fuel consumption by every topology with multiple PGs is lower than that consumed by the 1PG topology at the expense of a small increase in the equivalent fuel consumption. In other words, for a maximum of 1.6% higher discharged battery, the topologies with multiple PGs consume up to 67 g less engine fuel.

Fig. 5 summarises the best total fuel consumption, fuel economy, and reduction in total fuel consumption by 1PG, 2PG, and 3PG topologies. As 2PG-1 and 3PG-2 are the best topologies with respect to fuel consumption, the remaining analysis in this section focuses on these cases. As shown in Fig. 5, the rate of reduction of fuel consumption decreases when the number of PGs increases from two to three. It is hypothesised that further increasing the number of PGs from three to four would lead to a saturation in the reduction of the total fuel consumption.

Fig. 6(a) shows the evolution of the total fuel consumption of the 2PG-1 and 3PG-2 topologies over the US06 drive cycle as compared to 1PG-1 topology. Fig. 6(b) shows that the fuel consumed by the engine is independent of the topology during the $200-500$ s time interval, whilst it is much lower for the 2PG-1 and 3PG-2 topologies (especially the former) during the 0–180 s and 500–600 s time intervals. On the other hand, equivalent fuel consumption of 1PG-1 and 2PG-1 topologies are similar and higher than that of the 3PG-2 topology during the 200–500 s time interval. This is a similar trend to the one observed for the battery SoC in Fig. 6(c).

The main reasons for the reduction of fuel consumption of the 2PG and 3PG topologies are: (i) the speed of electric motors is higher with multiple PG topologies, leading to lower power demand from the engine; and (ii) fixed-gear ratio topologies save the electric power losses resulting from regulating the engine speed. These reasons are explained in more details in the remainder of this section.

As shown in Table 2, 1PG-1 and 2-PG-1 topologies can generate up to four modes whilst the 2PG-2, 3PG-1 and 3PG-2 topologies can generate five, seven and eight modes, respectively. 3PG-2 topology realise mode 1, mode 4, and mode 3 by engaging only one clutch (CL_1), which significantly reduces frequent clutch engagement and disengagement compared to other topologies. Fig. 7 shows that the EMS never chooses modes 8 or 9 for any of the topologies. Mode 8 (series mode) can only be selected when the battery $SoC \leq 40\%$, which never happens for the entire US06 drive cycle. The EMS does not select mode 9 because MG1 is used as a speed controller for the engine, and therefore MG1 and engine are not allowed to simultaneously provide torque to the wheels.

Fig. 7 shows that the EMS chooses mode $\in \{1,3,4\}$ for 1PG-1 and 2PG-1 topologies and mode $\in \{1,2,3,4,6,7\}$ for 3PG-2 during the 0–180 s and 500–600 s time intervals. Modes 1 and 4 are EV modes (see Table 2), where the former uses both MGs and the latter only MG2 to provide torque to the wheels. Conversely, all drivetrains contribute to the wheel torque in input-split mode 3, with the engine speed being regulated by the speed of MG1. Modes 2, 6 and 7 represent parallel topologies with a fixed ratio between the engine speed and the vehicle speed. However, unlike mode 4, mode 2 utilises only one MG.

Unlike in 1PG topology, the speed of MG2 in all modes of 2PG-1 and 3PG-2 other than mode 7 for 3PG-2 topologies are larger than the speed of final drive, with a coefficient of $\frac{R_2}{S_2} > 1$ for 2PG-1 and $1 + \frac{R_3}{S_3} > 1$ for 3PG-2 topologies. For example, given the gear ratio in Table 1, the speed of MG2 in 2PG-1 topology over the US06 drive cycle is up to 2.6 times higher than the speed of MG2 in 1PG-1 topology (see Fig. 8(a)). Moreover, Fig. 8(b) shows that the engine in 2PG-1 and 3PG-2 topologies rotates closer to its optimal speed (2050 rpm, as stated in Table 1) because of the higher speed of MG2, whilst engine speed

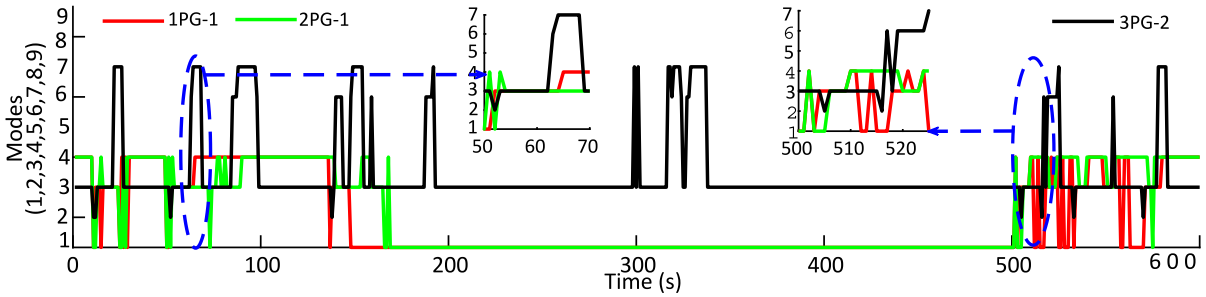

Fig. 7. The optimal mode selection by the EMS for different topologies.

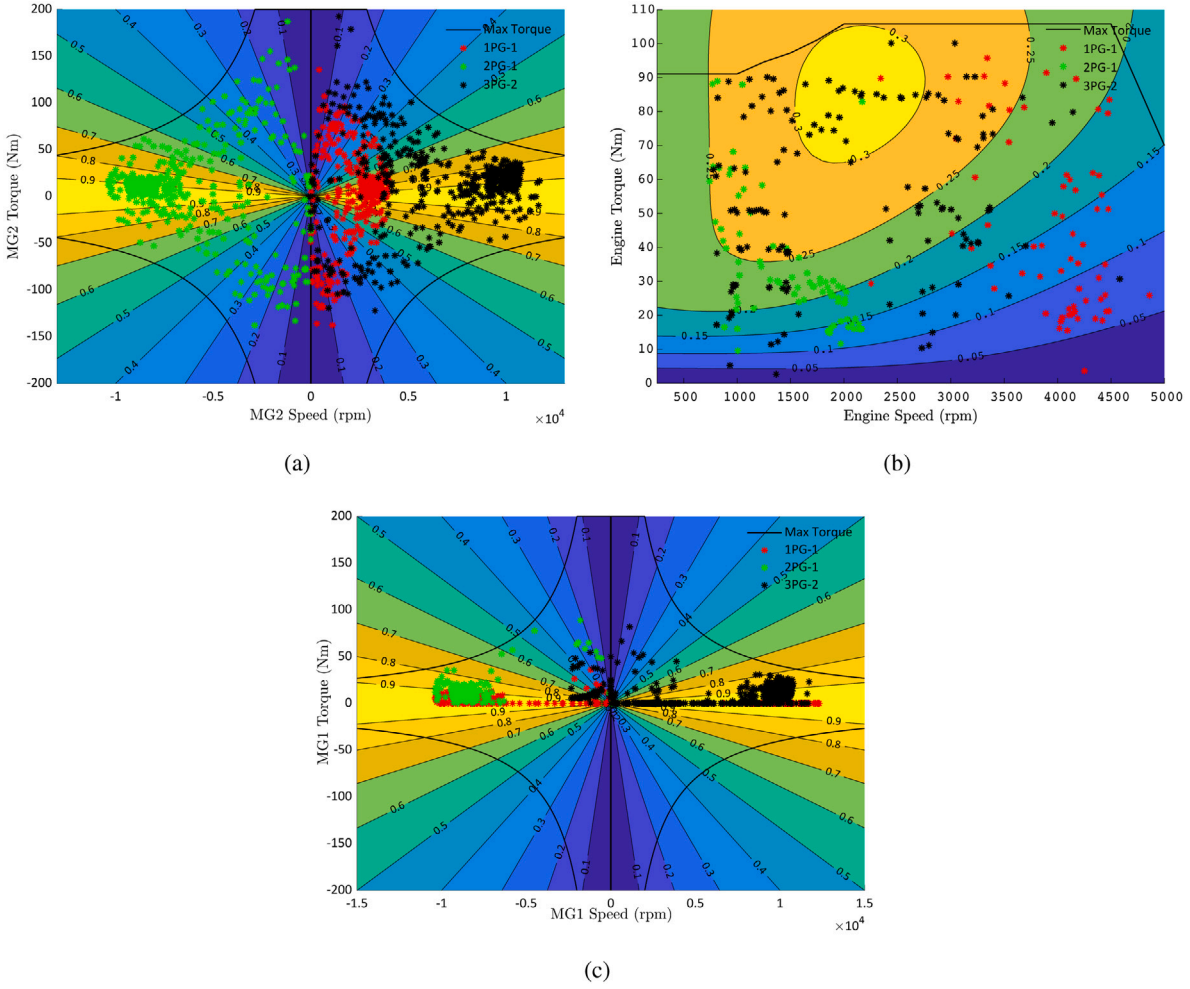

Fig. 8. Operating points of (a) MG2, (b) engine and (c) MG1 for the 1PG-1, 2PG-1 and 3PG-2 topologies.

is too high in 1PG-1 topology. Fig. 8(c) shows that there is not much difference in MG1 operation across the different topologies. For more details, please refer to Appendix A.

The higher speed of MG2 enables the engine to operate at high power with higher efficiency due to the shape of the efficiency map in Fig. 8(a). Therefore, the EMS utilises MG2 at higher power and efficiency for the 2PG and 3PG topologies than for the 1PG topology, as can be observed in Figs. 9(a) and 9(b). This will also reduce the required power from the engine and hence the direct fuel consumption (see Fig. 9(c)). This is shown in Fig. 8(b), where the brake specific fuel consumption (bsfc) of the engine of the 2PG-1 and 3PG-2 topologies is compared against that of the 1PG topology. This is at the expense of degrading the efficiency of MG1 for a similar delivered power (see Fig. 9(f)). However, MG1 does not contribute to the wheel torques during the 0–180 s and 500–600 s time intervals, and hence such efficiency reduction comprises an insignificant drawback.

As discussed before and shown in Fig. 5, increasing the number of PGs from two to three further reduces the total fuel consumption by an extra 1.5%. This is partially because the speed of MG2 in 3PG-2 topology can be even larger than in 2PG-1 (see Fig. 8(a)), resulting in MG2 being able to provide more power with high efficiency than 2PG-1.

However, the main reason for this is the availability and selection of the fixed-gear modes (i.e. modes 2 and 6), as shown in Fig. 7. The fixed-gear modes reduce equivalent energy consumption by not requiring MG1 to regulate the engine speed, hence excluding the corresponding losses [12]. During the 80–100 s, 170–180 s and 295–345 s time intervals, the EMS of the 3PG-2 topology chooses these fixed-gear modes whereas

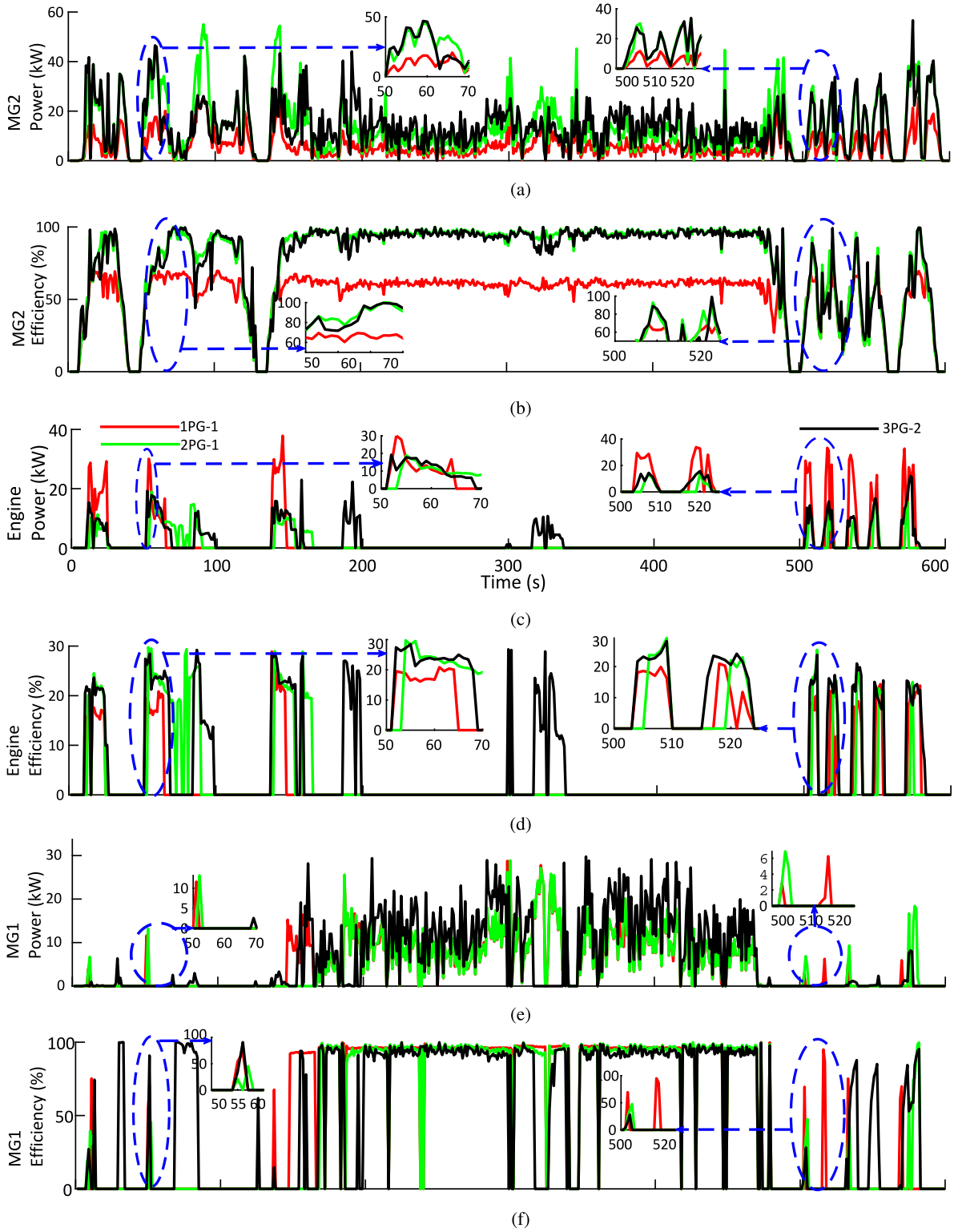

Fig. 9. Real-time simulation results for all five topologies, including (a) MG2 power, (b) MG2 efficiency (c) Engine power, (d) Engine efficiency (e) MG1 power, (f) MG1 efficiency.

other topologies with one and two PGs operate in 2EV mode (mode 1) as they do not support fixed-gear ones. Furthermore, in mode 7 (only available for 3PG-2 topology), the speeds of all components are the same and proportional to the vehicle speed (see Appendix A). The EMS uses this mode to reduce direct fuel consumption whenever there is a demand for high torque at low vehicle speed.

5. Conclusions

This work systematically analysed the effects on energy consumption of the number of planetary gears in the transmission system of hybrid electric powertrains. Thus, the minimum energy consumption of five hybrid topologies with one, two, and three PGs were compared over the US06 drive cycle. For each topology, an EMS ensured that the

combination of clutch engagements, torque distributions and components' speeds is such that it minimises the total energy consumption. The latter is calculated as the sum of the engine fuel consumption and the equivalent fuel consumption of the battery's discharge energy.

The incorporation of mode selection via clutch engagements into the nonlinear EMS led to a mixed-integer problem, which was then converted into a complementarity constrained problem, and solved using KNITRO within Neos server.

Real-time simulation results showed that increasing the number of PGs from one to two and from two to three reduces the total fuel consumption by 5% and 1.5%, respectively. The primary reason for lower fuel consumption is the higher power provided by the primary electric motor (MG2). Additional PGs help MG2 to operate at higher speed, where it can provide more power with higher efficiency. This also reduces the power required from the engine, resulting in lower engine fuel consumption. 3PG topologies also benefit from the availability of fixed gear modes, in which MG1 is not involved in regulating the engine speed, therefore avoiding the corresponding power loss.

To summarise, increasing the number of PGs reduces total fuel consumption due to the higher rotational speed of MG2 and to the availability of fixed gear modes. However, it is important to note that the rate at which total fuel consumption reduces seems to stagnate as the number of PGs increases.

The methodology developed for this systematic analysis can be applied to different types of electrified powertrains and drive cycles. However, it should be noted that mechanical losses, frictional losses, and the added cost and weight of the powertrains due to increasing the number of PGs were not considered in this study.

CRediT authorship contribution statement

Daizy Rajput: Original draft written, Conceptualization carried out, Methodology, Investigation, Formal analysis, Writing – review and editing, Project administration, Software. **Jose M. Herreros:** Investigation, Formal analysis, Funding acquisition, Supervision, Writing – review and editing. **Mauro S. Innocente:** Investigation, Formal analysis, Resources, Funding acquisition, Supervision, Writing – review and editing. **Jeremy Bryans:** Supervision, Writing – review and editing. **Joschka Schaub:** Formal analysis, Resources, Supervision. **Arash M. Dizqah:** Conceptualization carried out, Methodology, Investigation, Formal analysis, Funding acquisition, Supervision, Writing – review and editing, Project administration, Software.

Declaration of competing interest

The authors declare that they have no known competing financial interests or personal relationships that could have appeared to influence the work reported in this paper.

Acknowledgement

This work is funded by both coventry university and FEV, Europe GmbH, grant number 90440-01. All authors have read and agreed to the published version of the manuscript.

Appendix A. Multi-mode constraints of the developed EMS for different gearboxes

The constraints in Eqs. (19)–(23) show the distribution of torque at every mode for 1PG-1, 2PG-1, 2PG-2, 3PG-1, and 3PG-2 respectively.

1PG-1

$$T_{mg2_k} = \left(\frac{-T_{mg1_k} R_1}{S_1}\alpha_k + \frac{T_{req_k}}{D_{GR}}\right) m_{1,k} \tag{19a}$$

$$T_{mg1_k} = -S_1\left(\frac{T_{e_k}}{R_1 + S_1}\right) m_{2,k} \tag{19b}$$

$$\omega_{mg1_k} = \frac{R_1}{S_1}\omega_{mg2_k} m_{1,k}\alpha_k \tag{19c}$$

$$T_{mg2_k} = \frac{T_{req_k}}{D_{GR}} m_{2,4,k} \tag{19d}$$

$$T_{mg2_k} = -R_1\left(\frac{T_{e_k}}{R_1 + S_1}\alpha_k + \frac{T_{req_k}}{D_{GR}}\right) m_{3,k} \tag{19e}$$

$$T_{e_k} = T_{mg1_k} m_{8,k} \tag{19f}$$

$$\omega_{mg2_k} = D_{GR}\frac{V_{veh_k}}{r_{tyre}} m_{1,2,3,4,k} \tag{19g}$$

$$\omega_{e_k} = \left(\frac{\omega_{mg1_k}}{1 + \frac{R_1}{S_1}} + \frac{\omega_{mg2_k}}{1 + \frac{S_1}{R_1}}\right) m_{3,k}\alpha_k \tag{19h}$$

$$\omega_{e_k} = \left(\frac{\omega_{mg1_k}}{1 + \frac{R_1}{S_1}}\right) m_{2,k} \tag{19i}$$

$$\omega_{mg1_k} = \omega_{e_k}\left(S_1 + \frac{R_1}{S_1}\right) m_{8,k} \tag{19j}$$

2PG-1

$$T_{mg1_k} = \frac{S_1}{R_1}\left(-\frac{R_2}{S_2} T_{mg2_k}\alpha_k + \frac{T_{req_k}}{D_{GR}}\right) m_{1,k} \tag{20a}$$

$$T_{mg1_k} = -S_1\left(\frac{T_{e_k}}{R_1 + S_1}\right) m_{2,k} \tag{20b}$$

$$\omega_{mg1_k} = \left(\frac{S_2}{S_1}\right)\omega_{mg2_k} m_{1,k}\alpha_k \tag{20c}$$

$$T_{mg2_k} = \frac{S_2}{R_2}\frac{T_{req_k}}{D_{GR}} m_{2,4,k} \tag{20d}$$

$$T_{mg2_k} = \frac{S_2}{R_2}\left(-R_1\frac{T_{e_k}}{R_1 + S_1}\alpha_k + \frac{T_{req_k}}{D_{GR}}\right) m_{3,k} \tag{20e}$$

$$T_{e_k} = T_{mg1_k} m_{8,k} \tag{20f}$$

$$\omega_{mg2_k} = -\frac{R_2}{S_2}\frac{D_{GR}}{r_{tyre}} V_{veh_k} m_{1,2,3,4,k} \tag{20g}$$

$$\omega_{e_k} = \left(\frac{\omega_{mg1_k} S_1}{R_1 + S_1} - \frac{\omega_{mg2_k} S_2}{R_2 + S_2}\right) m_{3,k}\alpha_k \tag{20h}$$

$$\omega_{e_k} = \left(\frac{\omega_{mg1_k}}{1 + \frac{R_1}{S_1}}\right) m_{2,k} \tag{20i}$$

$$\omega_{mg1_k} = \omega_{e_k}\left(S_1 + \frac{R_1}{S_1}\right) m_{8,k} \tag{20j}$$

2PG-2

$$T_{mg2_k} = \frac{S_2}{R_2 + S_2}\left(-T_{mg1_k}\frac{R_1 + S_1}{S_1}\alpha_k + \frac{T_{req_k}}{D_{GR}}\right) m_{1,k} \tag{21a}$$

$$T_{mg2_k} = \frac{S_2}{R_2 + S_2}\left(-T_{e_k}\frac{R_1 + S_1}{R_1}\alpha_k + \frac{T_{req_k}}{D_{GR}}\right) m_{2,k} \tag{21b}$$

$$T_{mg2_k} = \frac{S_2}{R_2 + S_2}\left(-T_{e_k}\alpha_k - T_{mg1_k}\alpha_k + \frac{T_{req_k}}{D_{GR}}\right) m_{3,5,k} \tag{21c}$$

$$T_{mg2_k} = \frac{S_2}{R_2 + S_2}\frac{T_{req_k}}{D_{GR}} m_{4,k} \tag{21d}$$

$$\omega_{mg2_k} = \left(\frac{R_2+S_2}{S_2}\right) D_{GR} \frac{V_{veh_k}}{r_{tyre}} m_{1,2,3,4,k} \tag{21e}$$

$$\omega_{mg2_k} = \left(\frac{R_2+S_2}{S_2}\right) D_{GR} \frac{V_{veh_k}}{r_{tyre}} - \frac{S_1}{S_2}\omega_{mg1_k} m_{5,k}\alpha_k \tag{21f}$$

$$\omega_{mg1_k} = \left(\frac{R_1+S_1}{S_1}\right) D_{GR} \frac{V_{veh_k}}{r_{tyre}} m_{1,k}\alpha_k \tag{21g}$$

$$\omega_{e_k} = \left(\frac{R_2+S_2}{R_1}\right) D_{GR} \frac{V_{veh_k}}{r_{tyre}} m_{2,k}\alpha_k \tag{21h}$$

$$\omega_{e_k} = \left(\frac{R_2+S_2}{R_1}\right) D_{GR} \frac{V_{veh_k}}{r_{tyre}} + \frac{S_1}{R_1}\omega_{mg1_k} m_{3,5,k}\alpha_k \tag{21i}$$

3PG-1

$$T_{mg2_k} = \left(-T_{mg1_k}\alpha_k + \frac{T_{req_k}}{D_{GR}} \frac{S_3}{(R_3+S_3)}\right) m_{1,k} \tag{22a}$$

$$T_{mg2_k} = \left(-T_e\alpha_k + \frac{T_{req_k}}{D_{GR}} \frac{S_3}{(R_3+S_3)}\right) m_{2,3,6,k} \tag{22b}$$

$$T_{mg2_k} = \frac{T_{req_k}}{D_{GR}} \frac{S_3}{(R_3+S_3)} m_{4,k} \tag{22c}$$

$$\omega_{mg2_k} = \left(\frac{R_3+S_3}{S_3}\right) D_{GR} \frac{V_{veh_k}}{r_{tyre}} m_{1,2,4,6,k} \tag{22d}$$

$$\omega_{mg2_k} = D_{GR} \frac{V_{veh_k}}{r_{tyre}} \frac{R_1}{S_2}\omega_{mg1_k} m_{3,k} \tag{22e}$$

$$\omega_{mg1_k} = D_{GR} \frac{V_{veh_k}}{r_{tyre}} m_{1,6,k}, i \tag{22f}$$

$$\omega_{mg1_k} = \frac{R_2}{S_2} D_{GR} \frac{V_{veh_k}}{r_{tyre}} m_{2,k}, i \tag{22g}$$

$$\omega_{e_k} = \frac{R_2+S_2}{R_2}\omega_{mg1_k} m_{6,k}, \alpha_k \tag{22h}$$

$$\omega_{e_k} = \frac{R_2}{S_2}\frac{R_2+S_2}{R_2}\omega_{mg1_k} m_{2,k}, \alpha_k \tag{22i}$$

$$\omega_{e_k} = \omega_{mg2_k} m_{3,k}\alpha_k \tag{22j}$$

3PG-2

$$T_{mg2_k} = \left(-T_{e_k}\frac{S_2}{R_2R_1}\alpha_k + \frac{T_{req_k}}{D_{GR}} \frac{S_3}{(R_3+1)}\right) m_{3,7,k} \tag{23a}$$

$$T_{mg2_k} = \left(-T_{e_k}\alpha_k + \frac{T_{req_k}}{D_{GR}} \frac{S_3}{(R_3+1)}\right) m_{2,k} \tag{23b}$$

$$T_{mg2_k} = \left(-T_{e_k}\frac{S_2}{R_2R_1}\alpha_k + \frac{T_{req_k}}{D_{GR}} \frac{S_3}{(R_3+1)}\right) m_{6,k} \tag{23c}$$

$$\omega_{mg2_k} = \left(\frac{R_3+S_3}{S_3}\right) D_{GR} \frac{V_{veh_k}}{r_{tyre}} m_{2,3,5,6,k} \tag{23d}$$

$$\omega_{e_k} = \frac{S_2}{R_2}\left(D_{GR}\frac{V_{veh_k}}{r_{tyre}}\frac{R_3+S_3}{S_3} + \omega_{mg1_k}\right) m_{3,k}\alpha_k \tag{23e}$$

$$\omega_{e_k} = \frac{S_2}{R_1R_2}\left(D_{GR}\frac{V_{veh_k}}{r_{tyre}}\frac{R_3+S_3}{S_3} + \omega_{mg2_k}\right) m_{6,k}\alpha_k \tag{23f}$$

$$\omega_{e_k} = \left(\frac{R_3}{R_3+S_3}\omega_{mg2_k} - \frac{S_1}{R_1}\omega_{mg1_k}\right) m_{2,k}\alpha_k \tag{23g}$$

$$\omega_{mg2_k} = \omega_{mg1_k} = \omega_{e_k} = D_{GR}\frac{V_{veh_k}}{r_{tyre}} m_{7,k}\alpha_k \tag{23h}$$

Appendix B. Mass flow rate of fuel injection to engine per cycle

The mass of fuel from engine is calculated by Eq. (12). The variable q used in that equation refers to mass flow rate of fuel per cycle which is modelled as a polynomial function of order 5 of engine torque (T_e) and engine speed (ω_e):

$$\begin{aligned} q = {} & p00 + \\ & p10\omega_{e_k} + p01T_{e_k} + \\ & p20\omega_{e_k}^2 + p11\omega_{e_k}T_{e_k} + p02T_{e_k}^2 + \\ & p30\omega_{e_k}^3 + p21\omega_{e_k}^2T_{e_k} + p12\omega_{e_k}T_{e_k}^2 + p03T_{e_k}^3 + \\ & p40\omega_{e_k}^4 + p31\omega_{e_k}^3T_{e_k} + p22\omega_{e_k}^2T_{e_k}^2 + p13\omega_{e_k}T_{e_k}^3 + p04T_{e_k}^4 + \\ & p50\omega_{e_k}^5 + p41\omega_{e_k}^4T_{e_k} + p32\omega_{e_k}^3T_{e_k}^2 + \\ & \quad p23\omega_{e_k}^2T_{e_k}^3 + p14\omega_{e_k}T_{e_k}^4 + p05\omega_{e_k}^5 \end{aligned} \tag{24}$$

where:

$$\begin{aligned} p00 &= 9.888\times10^{-1} \\ p10 &= 3.087\times10^{-4} \\ p02 &= 9.858\times10^{-3} \\ p30 &= 2.739\times10^{-11} \\ p21 &= 1.265\times10^{-8} \\ p12 &= 3.348\times10^{-7} \\ p13 &= 1.059\times10^{-11} \\ p04 &= 1.742\times10^{-6} \\ p50 &= 7.724\times10^{-19} \\ p41 &= 8.884\times10^{-18} \\ p32 &= 4.498\times10^{-15} \\ p23 &= 1.147\times10^{-13} \\ p14 &= -2.844\times10^{-12} \\ p05 &= -5.227\times10^{-9} \\ p01 &= -5.154\times10^{-2} \\ p20 &= -4.332\times10^{-8} \\ p11 &= -5.215\times10^{-5} \\ p03 &= -2.006\times10^{-4} \\ p40 &= -9.107\times10^{-15} \\ p31 &= -9.222\times10^{-13} \\ p22 &= -8.382\times10^{-11} \end{aligned} \tag{25}$$

References

[1] CO2 emission performance standards for new passenger cars and light commercial vehicles. Tech. Rep., Department of Transport, UK; 2020.

[2] Zhuang W, Zhang X, Peng H, Wang L. Simultaneous optimization of topology and component sizes for double planetary gear hybrid powertrains. Energies 2016;9(6):411.

[3] Zhuang W, Zhang X, Ding Y, Wang L, Hu X. Comparison of multi-mode hybrid powertrains with multiple planetary gears. Appl Energy 2016;178:624–32.

[4] Zhang X, Peng H, Sun J, Li S. Automated modeling and mode screening for exhaustive search of double planetary gear power split hybrid powertrains. American Society of Mechanical Engineers; 2014.

[5] Yang Y, Hu X, Pei H, Peng Z. Comparison of power-split and parallel hybrid powertrain architectures with a single electric machine: Dynamic programming approach. Appl Energy 2016;168:683–90.

[6] Zhang X, Li C-T, Kum D, Peng H. Prius$^+$ and Volt$^-$: Configuration analysis of power-split hybrid vehicles with a single planetary gear. 2012;61:3544–52.

[7] Zhuang W, (Eben) SL, Zhang X, Kum D, Song Z, Yin G, Ju F. A survey of powertrain configuration studies on hybrid electric vehicles. Appl Energy 2020;262:114553.

[8] Rajput D, Herreros JM, Innocente MS, Schaub J, Dizqah AM. Electrified powertrain with multiple planetary gears and corresponding energy management strategy. Vehicles 2021;3(3):341–56.

[9] Zhang X, Li SE, Peng H, Sun J. Efficient exhaustive search of power-split hybrid powertrains with multiple planetary gears and clutches. J Dyn Syst Meas Control 2015;137(12).

[10] Duhon AN, Sevel KS, Tarnowsky SA, Savagian PJ. Chevrolet volt electric utilization. SAE Int J Alternat Powertrains 2015;4(2):269–76.

[11] Biswas A, Anselma PG, Rathore A, Emadi A. Effect of coordinated control on real-time optimal mode selection for multi-mode hybrid electric powertrain, vol. 289. 2021, 116695.
[12] Grewe TM, Conlon BM, Holmes AG. Defining the general motors 2-mode hybrid transmission. SAE Technical Paper 2007-01-0273, 2007.
[13] Sorrentino M, Rizzo G, Arsie I. Analysis of a rule-based control strategy for on-board energy management of series hybrid vehicles. Control Eng Pract 2011;19(12):1433–41.
[14] Dizqah AM, Ballard BL, Blundell MV, Kanarachos S, Innocente MS. A non-convex control allocation strategy as energy-efficient torque distributors for on-road and off-road vehicles. Control Eng Pract 2020;95:104256.
[15] Nazari S, Siegel J, Stefanopoulou A. Optimal energy management for a mild hybrid vehicle with electric and hybrid engine boosting systems. IEEE Trans Veh Technol 2019;68(4):3386–99.
[16] Gupta V. Ecms based hybrid algorithm for energy management in parallel hybrid electric vehicles. HCTL Open Int J Technol Innov Res (IJTIR) 2015;14. 2321–1814.
[17] Paganelli G, Tateno M, Brahma A, Rizzoni G, Guezennec Y. Control development for a hybrid-electric sport-utility vehicle: strategy, implementation and field test results (I). In: Proceedings of the american control conference, vol. 2, 2001, p. 5064–5064.
[18] Paganelli G, Delprat S, Guerra T-M, Rimaux J, Santin J-J. Equivalent consumption minimization strategy for parallel hybrid powertrains. In: vehicular technology conference. IEEE 55th vehicular technology conference. VTC spring 2002 (cat. no. 02ch37367), vol. 4. IEEE; 2002, p. 2076–81.
[19] Sun C, Sun F, He H. Investigating adaptive-ECMS with velocity forecast ability for hybrid electric vehicles, vol. 185. 2017, p. 1644–53.
[20] Dagci OH, Peng H, Grizzle JW. Hybrid electric powertrain design methodology with planetary gear sets for performance and fuel economy. IEEE Access 2018;6:9585–602.
[21] Sarvaiya S, Ganesh S, Xu B. Comparative analysis of hybrid vehicle energy management strategies with optimization of fuel economy and battery life. Energy 2021;228:120604.
[22] Shi D, Liu S, Cai Y, Wang S, Li H, Chen L. Pontryagin's minimum principle based fuzzy adaptive energy management for hybrid electric vehicle using real-time traffic information. Appl Energy 2021;286:116467.
[23] Hu Y, Li W, Xu K, Zahid T, Qin F, Li C. Energy management strategy for a hybrid electric vehicle based on deep reinforcement learning. Appl Sci 2018;8(2):187.
[24] Zhou J, Xue S, Xue Y, Liao Y, Liu J, Zhao W. A novel energy management strategy of hybrid electric vehicle via an improved TD3 deep reinforcement learning. 2021;224:120118.
[25] Li W, Cui H, Nemeth T, Jansen J, Ünlübayir C, Wei Z, Feng X, Han X, Ouyang M, Dai H, Wei X, Sauer DU. Cloud-based health-conscious energy management of hybrid battery systems in electric vehicles with deep reinforcement learning. Appl Energy 2021;293:116977.
[26] Hu X, Zhang X, Tang X, Lin X. Model predictive control of hybrid electric vehicles for fuel economy, emission reductions, and inter-vehicle safety in car-following scenarios. Energy 2020;196:117101.
[27] Zhang H, Fan Q, Liu S, Li SE, Huang J, Wang Z. Hierarchical energy management strategy for plug-in hybrid electric powertrain integrated with dual-mode combustion engine. Appl Energy 2021;304:117869.
[28] Qin Y, Tang X, Liu T, Cao D. Distributed deep reinforcement learning-based energy and emission management strategy for hybrid electric vehicles. IEEE Trans Veh Technol 2021;70(10):9922–34.
[29] Tang X, Teng Liu JC, Pu H, Khajepour A. Double deep reinforcement learning-based energy management for a parallel hybrid electric vehicle with engine start–stop strategy. IEEE Trans Transp Electrifi 2022;8(1):1376–88.
[30] Zhuang W, Zhang X, Zhao D, Peng H, Wang L. Optimal design of three-planetary-gear power-split hybrid powertrains. 2016;17(2):299–309.
[31] Zhuang W, Zhang X, Li D, Wang L, Yin G. Mode shift map design and integrated energy management control of a multi-mode hybrid electric vehicle. Appl Energy 2017;204:476–88.